No cell is an island: circulating T cell:monocyte complexes are markers of immune perturbations

Authors: Julie G. Burel[1], Mikhail Pomaznoy[1], Cecilia S. Lindestam Arlehamn[1], Daniela Weiskopf[1], Ricardo da Silva Antunes[1], Yunmin Jung[2], Mariana Babor[1], Veronique Schulten[1], Grégory Seumois[1], Jason A. Greenbaum[1], Sunil Premawansa[3], Gayani Premawansa[4], Ananda Wijewickrama[5], Dhammika Vidanagama[6], Bandu Gunasena[7], Rashmi Tippalagama[8], Aruna D. deSilva[1,8], Robert H. Gilman[9,10], Mayuko Saito[11], Randy Taplitz[12], Klaus Ley[2], Pandurangan Vijayanand[1,13], Alessandro Sette[1,13], Bjoern Peters[1,13,*]

Affiliations:

[1]Division of Vaccine Discovery, La Jolla Institute for Immunology, La Jolla, CA, USA.

[2]Division of Inflammation Biology, La Jolla Institute for Immunology, La Jolla, CA, USA.

[3]Department of Zoology and Environment Science, Science Faculty, University of Colombo, Sri Lanka.

[4]North Colombo Teaching Hospital, Ragama, Sri Lanka.

[5]National Institute of Infectious Diseases, Gothatuwa, Angoda, Sri Lanka.

[6]National Tuberculosis Reference Laboratory, Welisara, Sri Lanka

[7]National Hospital for Respiratory Diseases, Welisara, Sri Lanka

[8]Genetech Research Institute, Colombo, Sri Lanka #present address: Dept of Paraclinical Sciences, Faculty of Medicine, General Sir John Kotelawala Defence University, Ratmalana, Sri Lanka.

[9]Johns Hopkins University Bloomberg School of Public Health, Baltimore, MD, USA.

[10]Universidad Peruana Caytano Hereida, Lima, Peru.

[11]Department of Virology, Tohoku University Graduate School of Medicine, Sendai, Japan.

24 [12]Division of Infectious Diseases and Global Public Health, University of California San Diego,
25 La Jolla, CA, USA.

26 [13]Department of Medicine, University of California San Diego, La Jolla, CA, USA.

27 *Correspondence to: Professor Bjoern Peters, La Jolla Institute for Immunology, 9420 Athena
28 Circle, La Jolla, CA 92037, USA; Tel: 858 752 6914; Fax: 858 752 6987; e-mail: bpeters@lji.org

29

Abstract:

Our results highlight for the first time that a significant proportion of cell doublets in flow cytometry, previously believed to be the result of technical artefacts and thus ignored in data acquisition and analysis, are the result of true biological interaction between immune cells. In particular, we show that cell:cell doublets pairing a T cell and a monocyte can be directly isolated from human blood, and high resolution microscopy shows polarized distribution of LFA1/ICAM1 in many doublets, suggesting *in vivo* formation. Intriguingly, T cell:monocyte complex frequency and phenotype fluctuate with the onset of immune perturbations such as infection or immunization, reflecting expected polarization of immune responses. Overall these data suggest that cell doublets reflecting T cell-monocyte *in vivo* immune interactions can be detected in human blood and that the common approach in flow cytometry to avoid studying cell:cell complexes should be re-visited.

42 **Introduction**

43 Communication between immune cells is a major component of immune responses, either directly
44 through cell-cell contacts or indirectly through the secretion of messenger molecules such as
45 cytokines. In particular, the physical interaction between T cells and antigen-presenting cells
46 (APCs) is critical for the initiation of immune responses. APCs such as monocytes can take up
47 debris from the extracellular environment, and will display fragments of it on their surface to T
48 cells, which can identify potentially harmful, non-self antigens. There is paucity of data regarding
49 T cell-APCs interactions in humans *in vivo*, but they appear to be highly diverse in terms of
50 structure, length and function, depending on the nature and degree of maturation of the T cell and
51 APC (Friedl & Storim, 2004).

52 Despite the importance of interactions between immune cells, many experimental techniques in
53 immunology specifically avoid studying cell:cell complexes. The most notable example for this is
54 in flow cytometry, in which cells are labeled with a panel of fluorochrome-conjugated antibodies,
55 and each cell is then individually hit by a laser and its corresponding fluorescence emission spectra
56 recorded. In this process, doublets (a pair of two cells) are routinely observed but are believed to
57 be the results of technical artefacts due to *ex vivo* sample manipulation and are thus usually
58 discarded, or ignored in data analysis (Kudernatsch, Letsch, Stachelscheid, Volk, &
59 Scheibenbogen, 2013).

60 Blood is the most readily accessible sample in humans with high immune cell content. We and
61 others have shown circulating immune cells contain critical information that can be used for
62 diagnostic-, prognostic- and mechanistic understanding of a given disease or immune perturbation
63 (Bongen, Vallania, Utz, & Khatri, 2018; Burel et al., 2018; Grifoni et al., 2018; Roy Chowdhury

64 et al., 2018; Zak et al., 2016). Thus, whereas blood does not fully reflect what is occurring in
65 tissues, it contains relevant immune information likely to be 'leaking' from the affected
66 compartment. However, the presence of dual-cell complexes (and their content) has never been
67 studied in the peripheral blood and in the context of immune perturbations. Monocytes are a
68 subtype of phagocytes present in high abundance in the peripheral blood, which play a critical role
69 in both innate and adaptive immunity (Jakubzick, Randolph, & Henson, 2017). In particular,
70 monocytes have the capacity to differentiate into highly specialized APCs such as macrophages or
71 myeloid DCs (Sprangers, de Vries, & Everts, 2016). More recently, it has been highlighted that
72 they might directly function as APCs and thus contribute to adaptive immune responses (Jakubzick
73 et al., 2017; Randolph, Jakubzick, & Qu, 2008).

74 We recently identified a gene signature in memory CD4+ T cells circulating in the peripheral blood
75 that distinguishes individuals with latent TB infection (LTBI) from uninfected individuals (Burel
76 et al., 2018). Surprisingly, this dataset also led to the discovery of a group of monocyte-associated
77 genes co-expressed in memory CD4+ T cells whose expression is highly variable across
78 individuals. We ultimately traced this discovery to a population of CD3+CD14+ cells that are not
79 single cells but T cell:monocyte complexes present in the blood and that can be detected following
80 immune perturbations such as disease or vaccination. The frequency and T cell phenotypes of these
81 complexes appear to be associated with the nature of pathogen or vaccine. Thus, studying these
82 complexes promises to provide insights into the impact of immune perturbation on APCs, T cells
83 and their interactions.

84

85 **Results**

86 Unexpected detection of monocyte gene expression in CD4+ memory T cells from human subjects.

87 We initially set out to investigate the inter-individual variability of gene expression within sorted
88 memory CD4+ T cells from our previously characterized cohort of individuals with latent
89 tuberculosis infection (LTBI) and uninfected controls (Burel et al., 2018). Within the 100 most
90 variable genes, we identified a set of 22 genes that were highly co-expressed with each other (22-
91 var set, **Figure 1 – source data 1**). Strikingly, many of the genes contained within the 22-var set
92 were previously described as being highly expressed in classical monocytes (and to a lower extent
93 non-classical monocytes) but not in T cells (**Figure 1B,** (Schmiedel et al., 2018)). In particular,
94 the 22-var set contained the commonly used monocyte lineage marker CD14, the enzyme
95 lysozyme LYZ and the S100 calcium binding proteins S100A8 and S100A9, which are known to
96 be extremely abundant in monocytes (**Figure 1B**). By examining the flow cytometry data that were
97 acquired during cell sorting and applying our memory CD4+ T cell gating strategy (**Figure 1 –**
98 **figure supplement 1**), we identified that indeed there was a subpopulation within sorted memory
99 CD4+ T cells that stained positive for CD14 (**Figure 1C**). More importantly, the proportion of
100 memory CD4+ T cells that were CD14+ was positively correlated with the 22-var set expression
101 (spearman correlation coefficient r=0.42, $p < 0.0001$, **Figure 1D**), suggesting that this cell subset
102 is responsible for the expression of the monocyte-associated genes identified in Figure 1A. The
103 CD14+ memory CD4+ T cell population has similar forward and side scatter (FSC/SSC) values to
104 other memory CD4+ T cells and was thus sorted along with conventional CD14- memory CD4+
105 T cells (**Figure 1 – figure supplement 2**). In particular, there was no indication that CD14+
106 memory CD4+ T cells were the product of a technical artefact, such as dead cells or a compensation
107 issue.

108 Distinct CD3+CD14+ cell populations are present in the monocyte vs. the lymphocyte size gate.

109 To further investigate the origin of the CD14+ T cell population, we analyzed our flow cytometry
110 data, this time not restricting to the compartment of sorted memory T cells, but looking at all cells.
111 When gating on live FSC/SSC (including both monocytes and lymphocytes) singlet cells, two
112 populations of CD3+CD14+ could be readily identified: CD3+CD14hi cells and CD3+CD14mid
113 cells (**Figure 1E**). CD3+CD14hi cells were predominantly contained within the monocyte size
114 gate, whereas CD3+CD14mid cells were contained within the lymphocyte size gate (**Figure 1F**).

115 CD3+CD14+ cells consist of T cells bound to monocytes or monocyte debris.

116 To better understand the nature of CD3+CD14+ cells, we aimed to visualize the distribution of
117 their markers using imaging flow cytometry. Live events were divided into monocytes (CD3-
118 CD14+), T cells (CD3+CD14-), CD3+CD14hi cells, and CD3+CD14mid cells (**Figure 2A**), and
119 a random gallery of images was captured for each population. As expected, monocytes and T cells
120 contained exclusively single cells that expressed either CD14 (monocytes) or CD3 (T cells),
121 respectively (**Figure 2B**, *first and second panel*). To our surprise, CD3+CD14hi cells contained
122 predominantly two cells, sometimes even three cells, but no single cells (**Figure 2B**, *third panel*).
123 The doublets (or triplets) always contained at least one CD14+ cell, and one CD3+ cell (**Figure**
124 **2B**, *third panel*). CD3+CD14mid cells contained predominantly single CD3+ cells, but also some
125 doublets of one CD3+ cell and one CD14+ cell, but with CD14 expression lower than average
126 monocytes (**Figure 2B**, *fourth panel*). The majority of CD3+ T cell singlets in the CD3+CD14mid
127 population, but not in the CD3+CD14- T cell population, contained CD14+ particles, often seen
128 at the periphery of the CD3+ T cell membrane (**Figure 2B-C**). Looking more closely at the CD14+
129 particles contained within the CD3+CD14mid population using confocal microscopy, they were

130 found to have size and shape similar to cell debris (**Figure 2D**). To confirm our initial observation,
131 we repeated the experiment with multiple individuals, and compared for each cell population the
132 aspect ratio and area from the brightfield parameter collected with the image stream. Doublets are
133 known to present a larger area but reduced aspect ratio, when compared to single cells. Thus, their
134 overall ratio (area vs aspect ratio) is greater than in single cells. As expected, the area vs aspect
135 ratio was significantly higher for CD3+CD14hi cells and CD3+CD14mid cells compared to single
136 monocytes and T cells, and events in these two cell populations were found predominantly in the
137 'doublet gate' (**Figure 2E-F**). CD3+CD14hi cells also had a significantly higher ratio compared
138 to CD3+CD14mid cells (**Figure 2F**).

139 Taken together, these results demonstrate that CD3+CD14hi cells are tightly bound T
140 cell:monocyte complexes, in such strong interaction that sample processing and flow cytometry
141 acquisition did not break them apart. Conversely, the CD3+CD14mid population appears to
142 predominantly consist of single CD3+ T cells with attached CD14+ cell debris. This conclusion is
143 further supported by CD3+CD14hi complexes being found in the monocyte size gate, whereas
144 CD3+CD14mid cells were falling into the lymphocyte size gate (**Figure 1F**).

145 <u>T cell:monocyte complexes are not the result of cryopreservation or PBMC isolation.</u>

146 Next, we sought to determine whether the physical association of T cells and monocytes within
147 the T cell:monocyte complexes was the result of random cellular proximity during *ex vivo* sample
148 manipulation, or if the complexes are originally present in peripheral blood. We could readily
149 detect T cell:monocyte complexes in freshly isolated PBMC, and at similar frequencies as the same
150 samples after cryopreservation (**Figure 2G**). In another set of samples, using red blood cell (RBC)
151 magnetic depletion (and thus minimal sample manipulation), we could successfully identify T

152 cell:monocyte complexes directly from whole blood at frequencies matching the same sample after
153 PBMC isolation (**Figure 2 - figure supplement 1**). Taken together these data rule out that the
154 PBMC sample preparation or cryopreservation could be responsible for T cell:monocyte
155 complexes formation and thus suggest their presence *in vivo* in peripheral blood.

156 <u>T cell:monocyte complexes show increased expression of adhesion molecules at their interface.</u>

157 During T cell recognition of epitopes on APCs such as monocytes, the two cells are known to form
158 an 'immune synapse' at their contact point, which is stabilized by key adhesion molecules such as
159 LFA1 on the T cell, and ICAM1 on the APC (Dustin, 2014). Upon interaction these two molecules
160 undergo a drastic redistribution by focusing almost exclusively at the cell:cell point of contact,
161 thus forming a 'ring' that can be visualized (Wabnitz & Samstag, 2016). To identify candidate
162 immunological synapses in T cell:monocyte complexes, we used high resolution Airyscan images
163 of sorted doublets (see **Figure 2 – figure supplement 2** for sorting strategy). Almost a third (thirty
164 out of 105, 29%) of doublets analyzed from three different individuals displayed accumulation and
165 polarization of ICAM1 and LFA1 at their interfaces (**Figure 2H**). The percentage of polarized
166 doublets ranged from 17 to 67% between the subjects. In seven doublets, CD3 also accumulated
167 together with LFA1 (**Figure 2 – figure supplement 3**). However, we did not find welldeveloped,
168 classical immunological synapses, defined by central accumulation of CD3 and LFA1 exclusion
169 from central region of a synapse (Monks, Freiberg, Kupfer, Sciaky, & Kupfer, 1998; Thauland &
170 Parker, 2010). Overall, this suggests that a significant fraction of the detected T cell:monocyte
171 complexes utilizes adhesion markers associated with T cell:APC synapse formation to stabilize
172 their interaction, but they do not appear to being currently undergoing active TCR signaling.

173 The frequency of T cell:monocyte complexes varies in the context of diverse immune
174 perturbations.

175 Next, we thought to examine whether the formation of T cell:monocyte complexes is dysregulated
176 following immune perturbations. In order to accurately assess and compare the frequency of
177 complexes between cells of different types across different donor cohorts, we need to take into
178 account that their frequency is dependent on the abundance of its two components. Indeed, in
179 healthy subjects, where we expect constant affinity between T cells and monocytes, we observed
180 that the frequency of CD3+CD14+ cells is a linear function of the product of singlet monocyte and
181 T cell frequencies (**Figure 3A**). To correct for this, we elected to express the abundance of T
182 cell:monocytes complexes as a constant of association Ka, where similarly to a constant of
183 chemical complex association, the frequency of T cell:monocyte complexes is divided by the
184 product of the frequency of both T cells and monocytes (**Figure 3B**). As T cell and monocyte
185 frequencies in the blood can fluctuate greatly during immune perturbations, the Ka is a more
186 accurate readout of the likelihood of T cell:monocyte complex formation as opposed to raw
187 frequencies.

188 We first investigated the T cell:monocyte Ka in the context of two diseases where monocytes are
189 known to be important, namely active tuberculosis (TB) infection and dengue fever. In the case of
190 TB, although macrophages are known to be the primary target for *Mycobacterium tuberculosis*
191 (Mtb) infection and replication, monocytes can also be infected and contribute to the inflammatory
192 response (Srivastava, Ernst, & Desvignes, 2014). In active TB subjects, we found a significant
193 decrease in T cell:monocyte Ka at 2 months post treatment (**Figure 3C**). At the time of diagnosis,
194 some subjects displayed a Ka much higher than any uninfected or LTBI individuals, but because
195 of the high heterogeneity within the active TB cohort, these differences did not reach statistical

196 significance (**Figure 3 – figure supplement 1**). Dengue virus predominantly infects monocytes in
197 the peripheral blood (Kou et al., 2008), and circulating monocyte infection and activation is
198 increased in dengue hemorrhagic fever (the more severe form of dengue fever) (Durbin et al.,
199 2008). In subjects with acute dengue fever from Sri Lanka, patients that developed hemorrhagic
200 fever had higher T cell:monocyte Ka upon hospitalization compared to healthy, previously infected
201 subjects (blood bank donors seropositive for dengue antibodies) (**Figure 3D**). In contrast, patients
202 with a less severe form of acute dengue infection showed no significant difference in T
203 cell:monocyte Ka compared to healthy, previously infected donors (**Figure 3D**).

204 To assess whether vaccination also impacted the formation of T cell:monocyte complexes, we
205 obtained samples from healthy adults that received the tetanus, diphtheria and pertussis (Tdap)
206 booster vaccination. We indeed observed a significantly higher T cell:monocyte Ka at three days
207 post boost compared to baseline (**Figure 3E**), but no significant changes at one, seven or fourteen
208 days post boost (**Figure 3 – figure supplement 2**). Taken together, these data confirm that
209 circulating T cell:monocyte complexes can be found directly *ex vivo* in different immune
210 perturbations, and their likelihood of formation is associated with clinical parameters such as
211 disease severity, and they fluctuate as a function of time post treatment and post vaccination.

212 <u>T cells with different phenotypes are found in T cell:monocyte complexes dependent on the nature</u>
213 <u>of the immune perturbation.</u>

214 Finally, we reasoned that if immune perturbations increase the formation of T cell:monocyte
215 complexes, then the nature of the T cells contained in the complexes could provide insights into
216 which T cells are actively communicating with monocytes *in vivo*. In particular, the T cell subsets
217 that will associate with an APC for the different perturbations studied above are expected to be

218 distinct, and thus their likelihood to form a complex with a monocyte might differ too. The Tdap
219 vaccine contains exclusively protein antigens and is known to elicit predominantly memory CD4+
220 T cell responses (da Silva Antunes et al., 2018). *Mtb* is a bacterial pathogen known to trigger strong
221 CD4+ responses (Lindestam Arlehamn et al., 2016) as opposed to dengue virus, which is a viral
222 antigen and thus expected to elicit CD8+ responses.

223 Similarly to global T cell:monocyte complexes (Figs. 3C-E), we calculated for each CD4/CD8 T
224 cell subset its constant of association Ka with monocytes. In subjects with active TB, the Ka
225 between monocytes and CD4+CD8+ (DPOS) T cells or CD4+ T cells was significantly higher
226 than for CD8+ T cells (**Figure 3F)** and both DPOS and CD4+ T cell:monocyte complexes had
227 higher Ka in active TB compared to dengue hemorrhagic fever (**Figure 3 – figure supplement 3**).
228 Dengue hemorrhagic fever showed a higher T cell:monocyte Ka for CD8+ over CD4+ cells
229 whereas Tdap day 3 post boost showed the opposite, with highest Ka for CD4+ over CD8+ cells
230 (**Figure 3F**). The CD8+ T cell:monocyte Ka was also higher in Dengue and active TB compared
231 to Tdap boost (**Figure 3 – figure supplement 3**). Thus, the magnitude of Ka in CD4+ vs CD8+ T
232 cell subsets matched what is expected based on the nature of immune perturbation. Interestingly,
233 for all three immune perturbations studied the highest Ka with monocytes across all T cell subsets
234 was for CD4CD8 (DNEG) T cells (**Figure 3D**), and this effect was most pronounced in dengue
235 (**Figure 3 – figure supplement 3**). These cells could constitute gamma-delta T cells that are known
236 to be strongly activated in the peripheral blood during acute dengue fever (Tsai et al., 2015).

237 In summary, these data indicate that the T cell subsets that are preferentially associated with
238 monocytes differ from their individual frequencies in PBMC, and follow different patterns in the
239 three systems studied, further supporting the notion that these complexes are not the result of
240 random association, and are specific to the nature of the immune perturbation.

241 **Discussion**

242 The unexpected detection of monocyte genes expressed in cells sorted for memory T cell markers
243 led to the discovery that a population of CD3+CD14+ cells exist within the 'live singlet' events
244 gate and that these cells are T cells that are tightly associated with monocytes, and less frequently,
245 with monocyte-derived debris. Their presence in freshly isolated cells and the fact that a significant
246 fraction of the complexes showed enriched expression for LFA1/ICAM1 adhesion molecules at
247 their interface, suggest that they are not the product of random association of cells during
248 processing, but represent true interactions that occurred *in vivo* prior to the blood draw. The
249 frequency of T cell:monocyte complexes fluctuated over time in the onset of immune perturbations
250 such as following TB treatment or Tdap boost immunization and correlated with clinical
251 parameters such as disease severity in the case of dengue fever. Furthermore, the T cell subset in
252 preferential association within the monocyte in a complex varies in function of the nature of the
253 immune perturbation.

254 Thus, circulating CD3+CD14+ complexes appear to be the result of *in vivo* interaction between T
255 cells and monocytes. Because cells are in constant motion in the bloodstream, it is possible that T
256 cell:monocyte complex formation does not initially occur in peripheral blood. While we cannot
257 exclude that this is the case, we consider it more likely that their formation occurs in tissues or
258 draining lymph nodes, and the complexes are then 'leaking' into the peripheral circulation. The
259 most studied physical interaction between T cells and monocytes is the formation of immune
260 synapses. We found that about a third of complexes displayed LFA1/ICAM1 mediated interaction
261 similarly to immune synapses, but no CD3 polarization. The immune synapse formation is a highly
262 diverse event in terms of length and structure (Friedl & Storim, 2004), so it is possible that not all
263 detected complexes are at the same stage in the interaction. In some complexes, the nature (and

264 structure) of the architectural molecules forming the cell:cell contact might differ from traditional
265 immune synapses, too. Studying the nature and physical properties of these interactions could
266 provide insights into how T cells and monocytes can physically interact. Additionally, because
267 monocytes are not the only cell type known to associate with T cells, we think the ability to form
268 complexes with T cells should not be restricted to monocytes, but could apply more broadly to any
269 APC. Thus, it is likely that other types of complexes pairing a T cell and other APCs such as B
270 cells or dendritic cells can be found in the peripheral blood.

271 Increased immune cell:cell interactions might not necessarily always correlate with onset of
272 immune perturbations. Nevertheless, our preliminary data suggest that determining the constant of
273 association Ka of the T cell:monocyte (and likely more broadly any T cell:APC) complexes can
274 indicate the presence of an immune perturbation to both clinicians and immunologists. In dengue
275 infected subjects, a higher T cell:monocyte Ka at time of admission was associated with dengue
276 hemorrhagic fever, the more severe form of disease. The distinction between hemorrhagic vs. non-
277 hemorrhagic fever may become clear only days into hospitalization, so the ability to discriminate
278 these two groups of individuals at the time of admission has potential diagnostic value. In the case
279 of active TB, subjects presented a very high variability at diagnosis that might reflect the diverse
280 spectrum associated with the disease (Pai et al., 2016), but for all subjects a significant decrease in
281 T cell:monocyte Ka was observed upon treatment. This could thus be a tool to monitor treatment
282 success and predict potential relapses. It will of course be necessary to run prospective trials to
283 irrefutably demonstrate that the likelihood of association between T cells and monocytes have
284 predictive power with regard to dengue disease severity or over the course of TB treatment.
285 Additionally, the T cell:monocyte Ka was increased three days following Tdap booster
286 vaccination. Therefore, in vaccine trials, it could be examined as an early readout to gauge how

287 well the immune system has responded to the vaccine. Finally, in apparently 'healthy' populations,
288 or those with diffuse symptoms, an unusually high T cell:monocyte Ka in an individual could be
289 used as an indicator of a yet to be determined immune perturbation.

290

291 Beyond detecting abnormal frequencies of T cell:monocyte complexes, characterizing the T cells
292 and monocytes in these complexes might provide insights into the nature of immune perturbation
293 and subsequent immune response based on which complexes were formed. Our data suggest that
294 there are drastic differences in terms of T cell subsets in the complexes. Despite their lower
295 frequency over CD4+ and CD8+ T cells in the peripheral blood, DNEG T cells show a clear
296 increased association with monocytes. Gamma-delta T cells constitute the majority of circulating
297 DNEG T cells in humans, and LFA1 dependent crosstalk between gamma-delta T cells and
298 monocytes has been shown to be important in the context of bacterial infections (Eberl et al., 2009),
299 which might be also generalized to viral infections. Thus, the DNEG T cell:monocyte complexes
300 might well represent a novel type of interaction between T cells and monocytes, not necessarily
301 involving classical alpha-beta T cells or involving the formation of 'traditional' immune synapses.
302 Aside from the enrichment for DNEG cells in T cell:monocyte complexes in all samples analyzed,
303 we also observed that CD4 vs CD8 phenotype of the T cell present in complexes depends on the
304 nature of the immune perturbation studied, and reflects the expected polarization of immune
305 responses. Thus, looking for additional characteristics from T cells and monocytes present in the
306 complexes, such as the expression of tissue homing markers, specific TCRs and their
307 transcriptomic profile might provide further information about the fundamental mechanisms
308 underlying immune responses to a specific perturbation.

309 Why were T cell:monocyte complexes not detected and excluded in flow cytometry based on
310 gating strategies to avoid doublets? Surprisingly, all usual parameters (pulse Area (A), Height (H)
311 and Width (W) from forward and side scatter) looked identical between T cell:monocyte
312 complexes and singlet T cells or monocytes. The only parameter that could readily distinguish
313 between intact CD3+CD14hi complexes and single T cells or monocytes was the brightfield area
314 parameter from the imaging flow cytometer, which is a feature absent in non-imaging flow
315 cytometry. Thus, it seems that gating approaches and parameters available in conventional flow
316 cytometry are not sufficient to completely discriminate tightly bound cell pairs from individual
317 cells.

318 Given that T cell:monocyte complexes are not excluded by conventional FACS gating strategies,
319 why were they not reported previously? Examining our own past studies, a major reason is that
320 lineage markers for T cells (CD3), B cells (CD19) and monocytes (CD14) are routinely used to
321 remove cells not of interest in a given experiment by adding them to a 'dump channel'. For
322 example, most of our CD4+ T cell studies have CD8, CD19 and CD14, and dead cell markers
323 combined in the same channel (Arlehamn et al., 2014; Burel et al., 2018). Other groups studying
324 e.g. CD14+ monocytes are likely to add CD3 to their dump channel. This means that complexes
325 of cells that have two conflicting lineage markers such as CD3 and CD14 will often be removed
326 from datasets early in the gating strategy. Additionally, the detection of complexes by flow
327 cytometry is not straightforward. In our hands, we have found that conventional flow analyzers
328 give low frequency of complexes and poor reproducibility in repeat runs. This is opposed to cell
329 sorters, presumably due to differences in their fluidics systems, which puts less stress on cells and
330 does not disrupt complexes as much. Both the routine exclusion of cell populations positive for

331 two conflicting lineage markers and the challenges to reproduce such cell populations on different
332 platforms has likely contributed to them not being reported.

333 Moreover, even if a panel allows for the detection of complexes, and there is a stable assay used
334 to show their presence, there is an assumption in the field that detection of complexes is a result
335 of experimental artefacts. For example, we found a report of double positive CD3+CD34+ cells
336 detected by flow cytometry in human bone marrow, which followed up this finding and found
337 them to be doublets using microscopy imaging. The authors concluded that these complexes are
338 the product of random association and should be ignored (Kudernatsch et al., 2013). Their
339 conclusion may well be true for their study, but it highlights a common conception in the field of
340 cytometry that pairs of cells have to be artefacts. Another study described CD3+CD20+ singlets
341 cells observed by flow cytometry as doublets of T cells and B cells, and also concluded them to be
342 a technical artefact, in the sense that these cells are not singlets double expressing CD3 and CD20
343 (Henry et al., 2010). In this case however, authors pointed out that 'Whether the formation of these
344 doublets is an artefact occurring during staining or is a physiologic process remains to be
345 determined' (Henry et al., 2010).

346

347 We ourselves assumed for a long time that we might have an artefact finding, but given the
348 persistent association of T cell:monocyte complexes frequency and phenotype with clinically and
349 physiologically relevant parameters, we came to a new conclusion: cells are meant to interact with
350 other cells. Thus, detecting and characterizing complexes of cells isolated from tissues and bodily
351 fluids, can provide powerful insights into cell:cell communication events that are missed when
352 studying cells as singlets only.

353

354 **Material and methods**

355 Ethics statement

356 Samples from TB uninfected individuals were obtained from the University of California, San
357 Diego Antiviral Research Center clinic (AVRC at UCSD, San Diego) and National Blood Center
358 (NBC), Ministry of Health, Colombo, Sri Lanka, in an anonymous fashion as previously described
359 (Burel et al., 2017). Samples from individuals with LTBI were obtained from AVRC at UCSD,
360 San Diego, and the Universidad Peruana Cayetano Heredia (UPCH, Peru). Longitudinal active TB
361 samples were obtained from National Hospital for Respiratory Diseases (NHRD), Welisara, Sri
362 Lanka. Dengue previously infected samples were obtained from healthy adult blood donors from
363 the National Blood Center (NBC), Ministry of Health, Colombo, Sri Lanka, in an anonymous
364 fashion as previously described (Weiskopf et al., 2013). Acute dengue fever samples were
365 collected at National Institute of Infectious Diseases, Gothatuwa, Angoda, Sri Lanka and the North
366 Colombo Teaching Hospital, Ragama, in Colombo, Sri Lanka. Longitudinal Tdap booster
367 vaccination samples were obtained from healthy adults from San Diego, USA. Ethical approval to
368 carry out this work is maintained through the La Jolla Institute for Allergy and Immunology
369 Institutional Review Board, the Medical Faculty of the University of Colombo (which served as a
370 National Institutes of Health–approved institutional review board for Genetech) and the John's
371 Hopkins School of Public Health Institutional Review Board (RHG holds dual appointment at
372 UPCH and JHU). All clinical investigations have been conducted according to the principles
373 expressed in the Declaration of Helsinki. All participants, except anonymously recruited blood
374 bank donors in Sri Lanka, provided written informed consent prior to participation in the study.

375 Subjects and samples

376 LTBI status was confirmed in subjects by a positive IFN-γ release assay (IGRA) (QuantiFERON-
377 TB Gold In-Tube, Cellestis or T-SPOT.TB, Oxford Immunotec) and the absence of clinical and
378 radiographic signs of active TB. TB uninfected control subjects were confirmed as IGRA negative.
379 Active Pulmonary TB was defined as those exhibiting symptoms of TB, and are positive by sputum
380 and culture as confirmed by the National Tuberculosis Reference Laboratory (NTRL, Welisara,
381 Sri Lanka). Sputum was further confirmed positive for TB by PCR at Genetech (Sri Lanka). Active
382 TB patients in this study were confirmed negative for HIV, HBV and HCV. Upon enrollment
383 within seven days of starting their anti-TB treatment, active TB patients provided their first blood
384 sample, followed by a second blood sample two months after initial diagnosis. Acute dengue fever
385 and previously infected samples were classified by detection of virus (PCR+) and/or dengue-
386 specific IgM and IgG in the serum. Laboratory parameters such as platelet and leukocyte counts,
387 hematocrit, hemoglobulin, AST, ALT and if applicable an ultrasound examination of the chest and
388 abdomen or an X-ray were used to further diagnose patients with either dengue fever (DF) or
389 dengue hemorrhagic fever (DHF), a more severe form of disease, according to WHO's guidelines.
390 Longitudinal Tdap booster vaccination samples were obtained from individuals vaccinated in
391 childhood, and boosted with the DTP vaccine Tdap (Adacel). Blood samples were collected prior,
392 one day, three days, seven days and fourteen days post boost. For all cohorts, PBMC were obtained
393 by density gradient centrifugation (Ficoll-Hypaque, Amersham Biosciences) from leukapheresis
394 or whole blood samples, according to the manufacturer's instructions. Cells were resuspended to
395 10 to 50 million cells per mL in FBS (Gemini Bio-Products) containing 10% dimethyl sulfoxide
396 (Sigma) and cryopreserved in liquid nitrogen.

397 <u>Flow cytometry</u>

398 Surface staining of fresh or frozen PBMC was performed as previously described in (Burel et al.,
399 2017). Briefly, cells were stained with fixable viability dye eFluor506 (eBiosciences) and various
400 combinations of the antibodies listed in **Table supplement 1** for 20min at room temperature.
401 Acquisition was performed on a BD LSR-I cell analyzer (BD Biosciences) or on a BD FACSAria
402 III cell sorter (BD Biosciences). Compensation was realized with single-stained beads (UltraComp
403 eBeads, eBiosciences) in PBS using the same antibody dilution as for the cell staining.

404 Imaging flow cytometry

405 For the visualization of CD3+CD14+ cells, frozen PBMC were thawed and stained with CD3-
406 AF488 and CD14-PE or CD14-AF647 (see Table supplement 1 for antibody details) as described
407 in the flow cytometry section above. After two washes in PBS, cells were resuspended to $10x10^6$
408 cells/mL in FACS buffer containing 5µg/mL Hoechst (Invitrogen) and 1µg/mL 7-AAD
409 (Biolegend) and stored at 4°C protected from light until acquisition. Acquisition was performed
410 with ImageStreamX MkII (Amnis) and INSPIRE software version 200.1.620.0 at 40X
411 magnification and the lowest speed setting. A minimum of 4,000 CD3+CD14+ events in focus
412 were collected. Data analysis was performed using IDEAS version 6.2.183.0.

413 Sample preparation for microscopy

414 For the visualization of LFA1/ICAM1 polarization on T cell:monocyte complexes, frozen PBMC
415 were thawed and resuspended in blocking buffer (2% BSA, 10mM EGTA, 5mM EDTA, 0.05%
416 Sodium Azide in 1X PBS) supplemented with 2ul of Trustain FcR blocking reagent (BioLegend)
417 for 10min on ice. Antibodies (anti-human CD3-AF488, CD14-BV421, ICAM1-AF568, LFA1-
418 CF633 or LFA1-AF647, see Table supplement 1 for antibody details) were added and incubated
419 for 20 min on ice, and then washed twice with FACS buffer (PBS containing 0.5% FBS and 2mM

420 EDTA, pH 8). Cells were fixed with 4% Paraformaldehyde, 0.4% Glutaldehyde, 10mM EGTA,
421 5mM EDTA, 0.05 Sodium Azide, 2% sucrose in PBS for 1 h on ice, and then washed twice with
422 MACS buffer. Cells were resuspended in 0.5-1mL of MACS buffer, and kept at 4°C until sorting.
423 Cell sorting was performed on a BD Aria III/Fusion cell sorter (BD Biosciences). CD3+CD14+,
424 CD3+CD14- T cells and CD14+CD3- monocytes were sorted (see gating strategy **Figure**
425 **supplement 1B**) and each separately plated on a well of a μ-Slide 8 Well Glass Bottom chamber
426 (Ibidi) that was freshly coated with poly-L-lysine (0.01%) for 30 min RT before use. For in-house
427 antibody labeling, an Alexa Fluor™ 568 antibody labeling kit and a Mix-n-Stain™ CF®633 Dye
428 antibody labeling kit (Sigma) were used according to manufacturer's protocols.

429 Microscopy

430 Airyscan images were taken with a Plan-Apochromat 63x/1.4 Oil DIC M27 objective with a 152
431 μm sized pinhole with master gain 800 using a Zeiss LSM 880 confocal microscopy equipped with
432 an Airyscan detector (Carl Zeiss). 4 laser lines at 405, 488, 561, and 633 nm and a filter set for
433 each line were used for taking 20-25 series of z-plane Airyscan confocal images with a step of
434 0.185μm or 0.247 μm for each channel. Pixel dwelling time was 2.33 μs and x and y step sizes
435 were 43nm. 3D-Airyscan processing was performed with the Zen Black 2.3 SP1 program. For
436 some images, Z-plane linear transitional alignment was done by using the Zen Blue 2.5 program.
437 Contrast of images for each fluorophores channel was adjusted based on FMO (Fluorescence
438 minus one) control samples that were prepared and taken on the same day of each experiments. To
439 visualize cell fragments, sorted CD3+CD14mid cells were immobilized using CyGel Sustain
440 (Abcam) according to manufacturer recommendations. Three dimensional rendering of cellular
441 fragments (**Figure 2D**) was created in Imaris 9.1 software (Bitplane).

442 Bulk memory CD4+ T cell sorting

443 Frozen PBMC were thawed and stained with fixable viability dye eFluor506 (eBiosciences) and
444 various combinations of the antibodies listed in **Table supplement 1** as described in the flow
445 cytometry section above. Memory CD4 T cell sorting (see gating strategy **Figure supplement 1A**)
446 was performed on a BD Aria III/Fusion cell sorter (BD Biosciences). 100,000 memory CD4+ T
447 cells were sorted into TRIzol LS reagent (Invitrogen) for RNA extraction.

448 RNA sequencing and analysis

449 RNA sequencing and analysis of memory CD4+ T cells from LTBI infected subjects was
450 performed as described in (Picelli et al., 2013; Seumois et al., 2016) and quantified by qPCR as
451 described previously (Seumois et al., 2012). 5 ng of purified total RNA was used for poly(A)
452 mRNA selection, full length reverse-transcription and amplified for 17 cycles, following the smart-
453 seq2 protocol (Picelli et al., 2013; Seumois et al., 2016). After purification with Ampure XP beads
454 (Ratio 0.8:1, Beckmann Coulter) and quantification (Picogreen assay, Invitrogen), 1ng of cDNA
455 was used to prepare a Nextera XT sequencing library with the Nextera XT DNA library preparation
456 and index kits (Illumina). Samples were pooled and sequenced using the HiSeq2500 (Illumina) to
457 obtain at least 12 million 50-bp single-end reads per library. The single-end reads that passed
458 Illumina filters were filtered for reads aligning to tRNA, rRNA, and Illumina adapter sequences.
459 The reads were then aligned to UCSC hg19 reference genome using TopHat (v 1.4.1) (Trapnell,
460 Pachter, & Salzberg, 2009), filtered for low complexity reads, and parsed with SAMtools (Li et
461 al., 2009). Read counts to each genomic feature were obtained using HTSeq-count program (v
462 0.6.0) (Anders, Pyl, & Huber, 2015) using the "union" option. Raw counts were then imported to

463 R/Bioconductor package DESeq2 (Love, Huber, & Anders, 2014) to identify differentially
464 expressed genes among samples.

465

466 **Acknowledgments**

467 We thank Dr Chery Kim and all present and past members at the flow cytometry core facility at
468 the La Jolla Institute for Immunology for assistance in cell sorting and technical discussion. We
469 thank Dr. Zbigniew Mikulski from the microscopy core at the La Jolla Institute for Immunology
470 for assistance and technical advice on microscopy imaging. We thank Yoav Altman at the Sanford
471 Burnham Prebys flow cytometry core for technical assistance with imaging flow cytometry. We
472 thank Dr. Joe Trotter from the R&D Advanced Technology Group at BD Biosciences for useful
473 technical discussion about cytometry instrument fluidic systems. Research reported in this
474 manuscript was supported by the National Institute of Allergy and Infectious Diseases division of
475 the National Institutes of Health under award number U19AI118626, R01AI137681,
476 HHSN272201400045C, S10OD021831 and S10OD016262. The content is solely the
477 responsibility of the authors and does not necessarily represent the official views of the National
478 Institutes of Health. Imaging flow cytometry was supported by the James B. Pendleton Charitable
479 trust.

480

481 **Authorship and conflict-of-interest statements:** conceptualization: J.G.B, M.P, C.L.A, M.B,
482 A.S and B.P; investigation: J.G.B, M.P, C.L.A, D.W, R.d.S.A, Y.J, V.S and G.S; resources: C.L.A,
483 J.A.G, S.P, G.P, A.W, D.V, B.G, R.T, A.D.S, R.H, M.S, R.T, K.L and P.V; writing (original draft
484 preparation): J.G.B and B.P; writing (review and editing): all authors; funding acquisition: A.S
485 and B.P. All authors declare no competing interests.

486

487 **Data deposition**

488 Sequencing data is accessible online through Gene Expression Omnibus (accession numbers
489 GSE84445 and GSE99373, https://www.ncbi.nlm.nih.gov/geo) and Immport (Study number
490 SDY820, http://www.immport.org). All other data is available in the main text or the
491 supplementary materials.
492
493

494 **References**

495

496 Anders, S., Pyl, P. T., & Huber, W. (2015). HTSeq--a Python framework to work with high-
497 throughput sequencing data. *Bioinformatics, 31*(2), 166-169.
498 doi:10.1093/bioinformatics/btu638

499 Arlehamn, C. L., Seumois, G., Gerasimova, A., Huang, C., Fu, Z., Yue, X., . . . Peters, B. (2014).
500 Transcriptional profile of tuberculosis antigen-specific T cells reveals novel
501 multifunctional features. *J Immunol, 193*(6), 2931-2940. doi:10.4049/jimmunol.1401151

502 Bongen, E., Vallania, F., Utz, P. J., & Khatri, P. (2018). KLRD1-expressing natural killer cells
503 predict influenza susceptibility. *Genome Med, 10*(1), 45. doi:10.1186/s13073-018-0554-1

504 Burel, J. G., Lindestam Arlehamn, C. S., Khan, N., Seumois, G., Greenbaum, J. A., Taplitz, R., . .
505 . Peters, B. (2018). Transcriptomic Analysis of CD4(+) T Cells Reveals Novel Immune
506 Signatures of Latent Tuberculosis. *J Immunol, 200*(9), 3283-3290.
507 doi:10.4049/jimmunol.1800118

508 Burel, J. G., Qian, Y., Lindestam Arlehamn, C., Weiskopf, D., Zapardiel-Gonzalo, J., Taplitz, R.,
509 . . . Peters, B. (2017). An Integrated Workflow To Assess Technical and Biological
510 Variability of Cell Population Frequencies in Human Peripheral Blood by Flow Cytometry.
511 *J Immunol, 198*(4), 1748-1758. doi:10.4049/jimmunol.1601750

512 da Silva Antunes, R., Babor, M., Carpenter, C., Khalil, N., Cortese, M., Mentzer, A. J., . . . Sette,
513 A. (2018). Th1/Th17 polarization persists following whole-cell pertussis vaccination
514 despite repeated acellular boosters. *J Clin Invest, 128*(9), 3853-3865.
515 doi:10.1172/jci121309

516 Durbin, A. P., Vargas, M. J., Wanionek, K., Hammond, S. N., Gordon, A., Rocha, C., . . . Harris,
517 E. (2008). Phenotyping of peripheral blood mononuclear cells during acute dengue illness
518 demonstrates infection and increased activation of monocytes in severe cases compared to
519 classic dengue fever. *Virology, 376*(2), 429-435. doi:10.1016/j.virol.2008.03.028

520 Dustin, M. L. (2014). The immunological synapse. *Cancer Immunol Res, 2*(11), 1023-1033.
521 doi:10.1158/2326-6066.cir-14-0161

522 Eberl, M., Roberts, G. W., Meuter, S., Williams, J. D., Topley, N., & Moser, B. (2009). A rapid
523 crosstalk of human gammadelta T cells and monocytes drives the acute inflammation in
524 bacterial infections. *PLoS Pathog, 5*(2), e1000308. doi:10.1371/journal.ppat.1000308

525 Friedl, P., & Storim, J. (2004). Diversity in immune-cell interactions: states and functions of the
526 immunological synapse. *Trends Cell Biol, 14*(10), 557-567. doi:10.1016/j.tcb.2004.09.005

527 Grifoni, A., Costa-Ramos, P., Pham, J., Tian, Y., Rosales, S. L., Seumois, G., . . . Sette, A. (2018).
528 Cutting Edge: Transcriptional Profiling Reveals Multifunctional and Cytotoxic Antiviral
529 Responses of Zika Virus-Specific CD8(+) T Cells. *J Immunol*.
530 doi:10.4049/jimmunol.1801090

531 Henry, C., Ramadan, A., Montcuquet, N., Pallandre, J. R., Mercier-Letondal, P., Deschamps, M.,
532 . . . Robinet, E. (2010). CD3+CD20+ cells may be an artifact of flow cytometry: comment
533 on the article by Wilk et al. *Arthritis Rheum, 62*(8), 2561-2563; author reply 2563-2565.
534 doi:10.1002/art.27527

535 Jakubzick, C. V., Randolph, G. J., & Henson, P. M. (2017). Monocyte differentiation and antigen-
536 presenting functions. *Nat Rev Immunol, 17*(6), 349-362. doi:10.1038/nri.2017.28

537 Kou, Z., Quinn, M., Chen, H., Rodrigo, W. W., Rose, R. C., Schlesinger, J. J., & Jin, X. (2008).
538 Monocytes, but not T or B cells, are the principal target cells for dengue virus (DV)
539 infection among human peripheral blood mononuclear cells. *J Med Virol, 80*(1), 134-146.
540 doi:10.1002/jmv.21051

541 Kudernatsch, R. F., Letsch, A., Stachelscheid, H., Volk, H. D., & Scheibenbogen, C. (2013).
542 Doublets pretending to be CD34+ T cells despite doublet exclusion. *Cytometry A, 83*(2),
543 173-176. doi:10.1002/cyto.a.22247

544 Li, H., Handsaker, B., Wysoker, A., Fennell, T., Ruan, J., Homer, N., . . . Durbin, R. (2009). The
545 Sequence Alignment/Map format and SAMtools. *Bioinformatics, 25*(16), 2078-2079.
546 doi:10.1093/bioinformatics/btp352

547 Lindestam Arlehamn, C. S., McKinney, D. M., Carpenter, C., Paul, S., Rozot, V., Makgotlho, E.,
548 . . . Sette, A. (2016). A Quantitative Analysis of Complexity of Human Pathogen-Specific
549 CD4 T Cell Responses in Healthy M. tuberculosis Infected South Africans. *PLoS Pathog,*
550 *12*(7), e1005760. doi:10.1371/journal.ppat.1005760

551 Love, M. I., Huber, W., & Anders, S. (2014). Moderated estimation of fold change and dispersion
552 for RNA-seq data with DESeq2. *Genome Biol, 15*(12), 550. doi:10.1186/s13059-014-
553 0550-8

554 Monks, C. R., Freiberg, B. A., Kupfer, H., Sciaky, N., & Kupfer, A. (1998). Three-dimensional
555 segregation of supramolecular activation clusters in T cells. *Nature, 395*(6697), 82-86.

556 Pai, M., Behr, M. A., Dowdy, D., Dheda, K., Divangahi, M., Boehme, C. C., . . . Raviglione, M.
557 (2016). Tuberculosis. *Nat Rev Dis Primers, 2*, 16076. doi:10.1038/nrdp.2016.76

558 Picelli, S., Bjorklund, A. K., Faridani, O. R., Sagasser, S., Winberg, G., & Sandberg, R. (2013).
559 Smart-seq2 for sensitive full-length transcriptome profiling in single cells. *Nat Methods,*
560 *10*(11), 1096-1098. doi:10.1038/nmeth.2639

561 Randolph, G. J., Jakubzick, C., & Qu, C. (2008). Antigen presentation by monocytes and
562 monocyte-derived cells. *Curr Opin Immunol, 20*(1), 52-60. doi:10.1016/j.coi.2007.10.010

563 Roy Chowdhury, R., Vallania, F., Yang, Q., Lopez Angel, C. J., Darboe, F., Penn-Nicholson, A.,
564 . . . Chien, Y. H. (2018). A multi-cohort study of the immune factors associated with M.
565 tuberculosis infection outcomes. *Nature, 560*(7720), 644-648. doi:10.1038/s41586-018-
566 0439-x

567 Schmiedel, B. J., Singh, D., Madrigal, A., Valdovino-Gonzalez, A. G., White, B. M., Zapardiel-
568 Gonzalo, J., . . . Vijayanand, P. (2018). Impact of Genetic Polymorphisms on Human
569 Immune Cell Gene Expression. *Cell*. doi:10.1016/j.cell.2018.10.022

570 Seumois, G., Vijayanand, P., Eisley, C. J., Omran, N., Kalinke, L., North, M., . . . Ansel, K. M.
571 (2012). An integrated nano-scale approach to profile miRNAs in limited clinical samples.
572 *Am J Clin Exp Immunol, 1*(2), 70-89.

573 Seumois, G., Zapardiel-Gonzalo, J., White, B., Singh, D., Schulten, V., Dillon, M., . . . Vijayanand,
574 P. (2016). Transcriptional Profiling of Th2 Cells Identifies Pathogenic Features Associated
575 with Asthma. *J Immunol, 197*(2), 655-664. doi:10.4049/jimmunol.1600397

576 Sprangers, S., de Vries, T. J., & Everts, V. (2016). Monocyte Heterogeneity: Consequences for
577 Monocyte-Derived Immune Cells. *J Immunol Res, 2016*, 1475435.
578 doi:10.1155/2016/1475435

579 Srivastava, S., Ernst, J. D., & Desvignes, L. (2014). Beyond macrophages: the diversity of
580 mononuclear cells in tuberculosis. *Immunol Rev, 262*(1), 179-192. doi:10.1111/imr.12217

581 Thauland, T. J., & Parker, D. C. (2010). Diversity in immunological synapse structure.
582 *Immunology, 131*(4), 466-472. doi:10.1111/j.1365-2567.2010.03366.x

583 Trapnell, C., Pachter, L., & Salzberg, S. L. (2009). TopHat: discovering splice junctions with
584 RNA-Seq. *Bioinformatics, 25*(9), 1105-1111. doi:10.1093/bioinformatics/btp120

585 Tsai, C. Y., Liong, K. H., Gunalan, M. G., Li, N., Lim, D. S., Fisher, D. A., . . . Wong, S. B. (2015).
586 Type I IFNs and IL-18 regulate the antiviral response of primary human gammadelta T
587 cells against dendritic cells infected with Dengue virus. *J Immunol, 194*(8), 3890-3900.
588 doi:10.4049/jimmunol.1303343

589 Wabnitz, G. H., & Samstag, Y. (2016). Multiparametric Characterization of Human T-Cell
590 Immune Synapses by InFlow Microscopy. *Methods Mol Biol, 1389*, 155-166.
591 doi:10.1007/978-1-4939-3302-0_10

592 Weiskopf, D., Angelo, M. A., de Azeredo, E. L., Sidney, J., Greenbaum, J. A., Fernando, A. N., .
593 . . Sette, A. (2013). Comprehensive analysis of dengue virus-specific responses supports
594 an HLA-linked protective role for CD8+ T cells. *Proc Natl Acad Sci U S A, 110*(22),
595 E2046-2053. doi:10.1073/pnas.1305227110

596 Zak, D. E., Penn-Nicholson, A., Scriba, T. J., Thompson, E., Suliman, S., Amon, L. M., . . .
597 Hanekom, W. A. (2016). A blood RNA signature for tuberculosis disease risk: a
598 prospective cohort study. *Lancet, 387*(10035), 2312-2322. doi:10.1016/s0140-
599 6736(15)01316-1

600

601 **Figure legends**

602 **Figure 1. Two cell populations expressing both T cell (CD3) and monocyte (CD14) surface**
603 **markers exist in the live singlet cell population of PBMC from human subjects.** A) The top
604 100 most variable genes in memory CD4+ T cells across TB uninfected (TBneg) and LTBI
605 infected subjects. B) Immune cell type specific expression of the 22-var genes identified in A).
606 Every bar consists of stacked sub-bars showing the TPM normalized expression of every gene in
607 corresponding cell type. Expression of genes for the blood cell types shown were taken from the
608 DICE database ((Schmiedel et al., 2018), http://dice-database.org/). C) Detection of CD14+ events
609 within sorted CD4+ memory T cells and D) non-parametric spearman correlation between their
610 frequency and the PC1 from the 22-var genes. E) Gated on 'singlet total live cells', two populations
611 of CD3+CD14+ cells can be identified based on the level of expression of CD14. F) Based on FSC
612 and SSC parameters, CD3+CD14hi cells are contained within the monocyte gate, whereas
613 CD3+CD14mid cells are contained within the lymphocyte gate. Data were derived from 30 LTBI
614 subjects and 29 TB uninfected control subjects.

615 **Figure 1 – figure supplement 1. Gating strategy to isolate bulk memory CD4+ T cells.**

616 **Figure 1 – figure supplement 2. Backgating of CD14+ cells within sorted memory CD4+ T**
617 **cells.**

618 **Figure 2. CD3+CD14+ cells are tightly bound T cell:monocyte complexes that represent *in***
619 ***vivo* association.** A) Gating strategy and B) random gallery of events for monocytes (CD14+CD3-
620), T cells (CD3+CD14-), CD3+CD14hi cells and CD3+CD14mid cells determined by imaging
621 flow cytometry (ImageStreamX, MkII Amnis Amnis). CD14+ cell debris were identified within
622 CD3+CD14mid cells C) by imaging flow cytometry and D) confocal microscopy after bulk

623 population cell sorting. E) Plots and F) Ratio of Aspect ratio vs Area of the brightfield parameter
624 for monocytes (CD14+CD3-), T cells (CD3+CD14-), CD3+CD14hi cells and CD3+CD14mid
625 cells, determined by imaging flow cytometry. G) Non-parametric Spearman correlation of the
626 frequency of live singlets CD3+CD14+ cells in paired fresh PBMC vs cryopreserved PBMC
627 derived from 45 blood draws of healthy subjects. H) Single z-plan (0μm) images (*left*) and z-plane
628 stacks (*right*) of the region marked (dashed rectangle) from one sorted CD3+CD14+ T
629 cell:monocyte complex displaying accumulation of LFA1 and ICAM1 at the interface. Images
630 show expression of CD14 (blue), CD3 (green), ICAM1(Cyan), and LFA1 (Magenta). Relative z-
631 positions are indicated on the right, and scale bars represent 2 μm. Imaging flow cytometry data
632 was derived from 10 subjects across three independent experiments and microscopy data was
633 representative of the analysis of n=105 CD3+CD14+ complexes isolated from 3 subjects across
634 three independent experiments.

635 **Figure 2 - figure supplement 1. Non-parametric spearman correlation between CD3+CD14+**
636 **frequencies in whole blood versus fresh PBMC.** Red blood cells were magnetically depleted
637 from fresh whole blood using the EasySep RBC depletion kit (STEMCELL technologies)
638 according to the manufacturer's instructions. Data was derived from 10 independent blood draws
639 of healthy subjects.

640 **Figure 2 – figure supplement 2. Gating strategy to isolate CD3+CD14+ cells.**

641 **Figure 2 - figure supplement 3. Accumulation of CD3, LFA1 and ICAM1 at the interface of**
642 **a T cell:monocyte complex.** Single z-plan (0μm) images (*left*) and z-plane stacks (*right*) of the
643 region marked (dashed rectangle) from one sorted CD3+CD14+ Tcell:monocyte complex
644 displaying accumulation of LFA1 and ICAM1 at the interface. Images show expression of CD14

645 (blue), CD3 (green), ICAM1(Cyan), and LFA1 (Magenta). Relative z-positions are indicated on
646 the right, and scale bars represent 2 μm.

647

648 **Figure 3. The constant of association Ka between monocytes and T cells (and T cell subsets)**
649 **varies with the presence and nature of immune perturbations.** A) Non-parametric spearman
650 correlation between the frequency of T cell:monocyte complexes and the product of singlet T cells
651 and monocyte frequencies in healthy subjects (n=59). B) Formula for the calculation of the T
652 cell:monocyte constant of association Ka. T cell:monocyte complexes constant of association Ka
653 in C) active TB subjects at diagnosis and 2 months post treatment (n=15), D) individuals with
654 acute dengue fever (n=18), acute dengue hemorrhagic fever (n=24) or previously infected (n=47)
655 and E) previously vaccinated healthy adults (n=16) before and three days post boost with Tdap
656 vaccine, calculated as explained in B). F) The constant of association Ka between monocytes and
657 T cell subsets in active TB subjects at diagnosis (n=25), individuals with acute dengue hemorrhagic
658 fever (n=24) and previously vaccinated healthy adults three days post boost with Tdap vaccine
659 (n=16), calculated as explained in B). Statistical differences over time and across cell populations
660 within subjects were determined using the non-parametric paired Wilcoxon test; other statistical
661 differences were determined using the non-parametric Mann-Whitney test; *, $p < 0.05$; **, $p <$
662 0.01; ***, $p < 0.01$; ****, $p < 0.0001$. Plots represent individual data points, median and
663 interquartile range across all subjects within each cohort. Raw frequencies of T cell:monocyte
664 complexes for the different disease cohorts are available on Figure 3 – figure supplement 3.

665

666 **Figure 3 – figure supplement 1. T cell:monocyte constant of association Ka in subjects with**
667 **active TB, latent TB or TB uninfected individuals.** T cell:monocyte constant of association Ka
668 for was calculated as explained in Fig. 3B from active TB samples (n=15) collected at diagnosis
669 from Sri Lanka, latent TB samples collected from subjects living in San Diego (n=22) or Peru
670 (n=8), and TB uninfected samples collected from subjects living in San Diego (n=29) or Sri Lanka
671 (n=14). Plots represent individual data points, median and interquartile range across all subjects
672 within each cohort.

673

674 **Figure 3 – figure supplement 2. T cell:monocyte constant of association Ka fluctuates as a**
675 **function of time following Tdap boost administration.** Previously vaccinated healthy subjects
676 (n=16) were re-immunized with Tdap and blood collected before, one day, three days, seven days
677 and fourteen days post boost. Plots represent the median and interquartile range across all 16
678 subjects. T cell:monocyte constant of association Ka was calculated as explained in Fig. 3B.

679

680 **Figure 3 – figure supplement 3. Comparison of constant of association Ka between**
681 **monocytes and T cell subsets across different immune perturbations.** Constant of association
682 Ka for each T cell subset and monocytes was calculated as explained in Fig. 3B from active TB
683 subjects at diagnosis (n=25), individuals with acute dengue hemorrhagic fever (n=24) and
684 previously vaccinated healthy adults three day post boost with Tdap vaccine (n=16). Plots
685 represent individual data points, median and interquartile range across all subjects.

686

687 **Figure 3 – figure supplement 4. Frequencies of T cell:monocyte complexes in different**
688 **immune perturbation models.** Frequencies of T cell:monocyte complexes (and T cell
689 subsets:monocyte complexes) expressed as percent of live cells were determined in active TB
690 subjects at diagnosis (n=25) and two months post treatment (n=15), individuals with acute dengue
691 hemorrhagic fever (n=24) and previously vaccinated healthy adults three days post boost with
692 Tdap vaccine (n=16). Statistical differences over time and across cell populations within subjects
693 were determined using the non-parametric paired Wilcoxon test; other statistical differences were
694 determined using the non-parametric Mann-Whitney test; *, $p < 0.05$; **, $p < 0.01$; ***, $p < 0.01$;
695 ****, $p < 0.0001$. Plots represent individuals data points, median and interquartile range across all
696 subjects within each cohort.

697 **Figure 1**

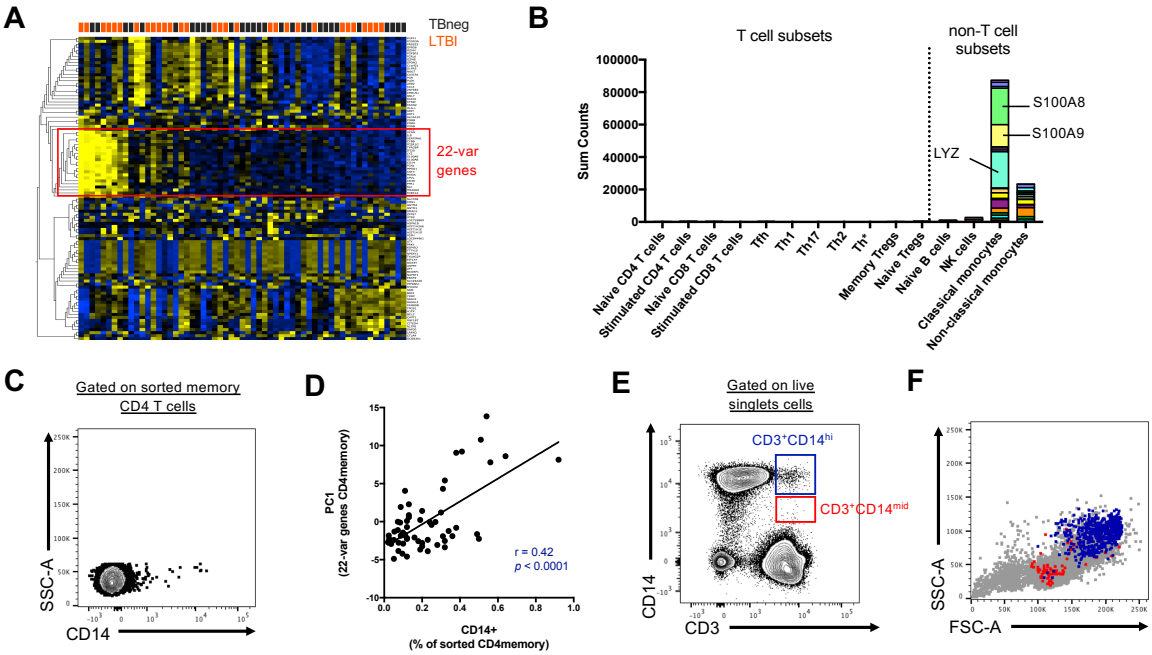

698

699

700 **Figure 1 – figure supplement 1**

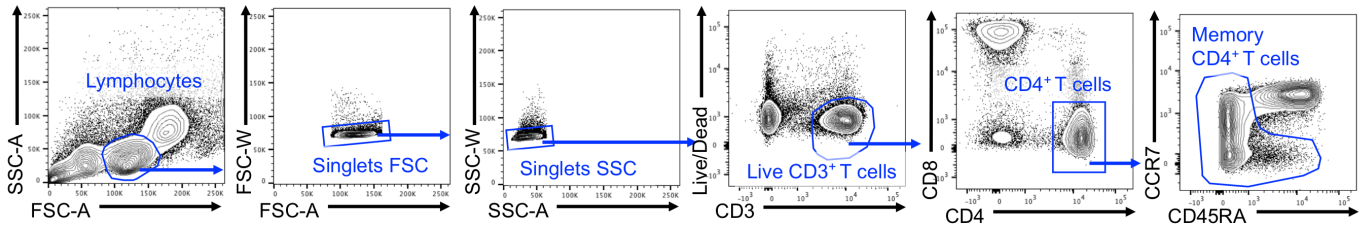

701

702

703 **Figure 1 – figure supplement 2**

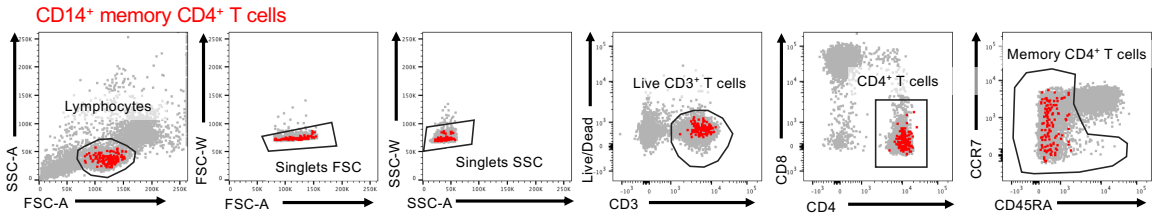

704

705 **Figure 2**

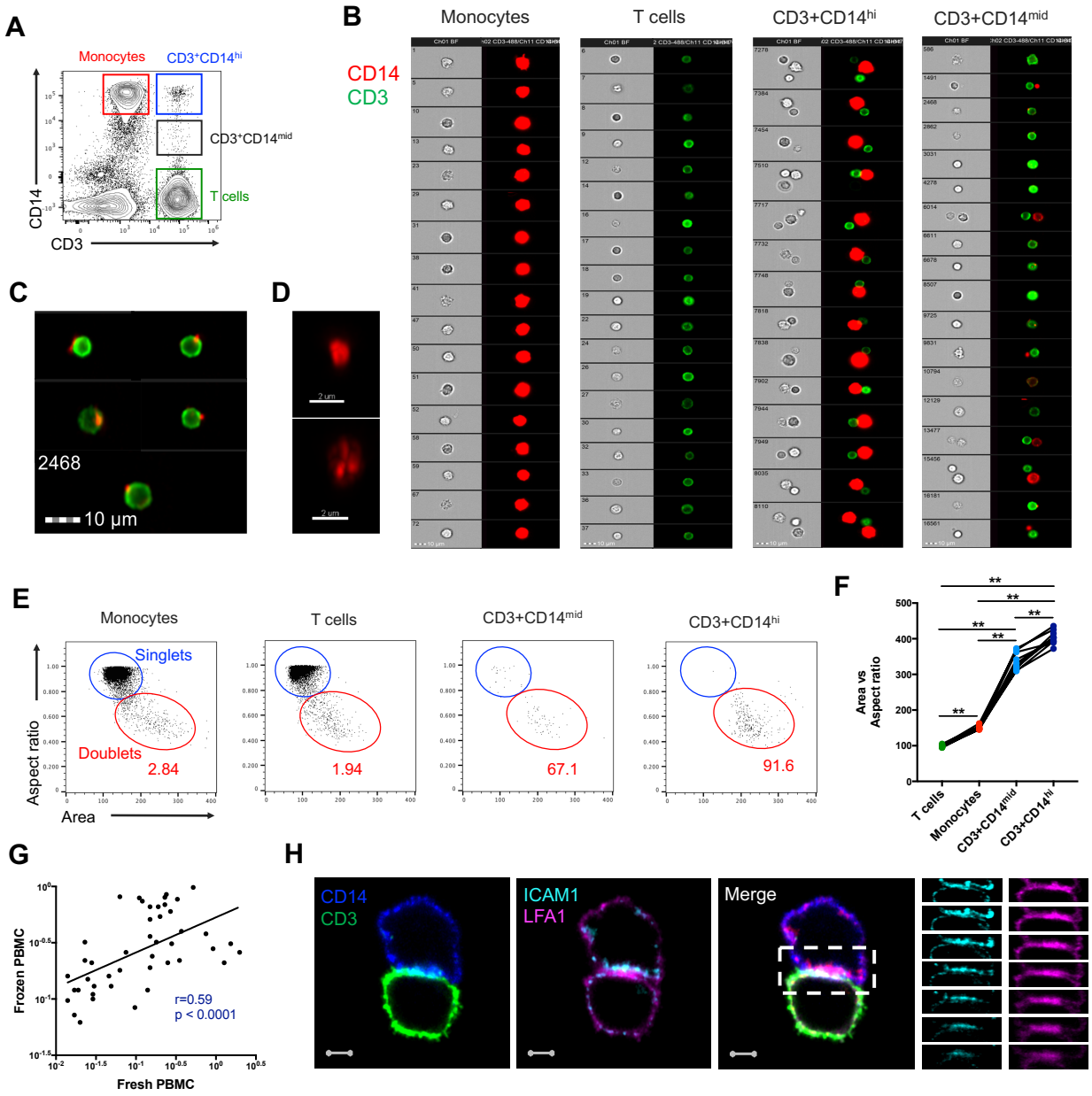

706

707

708 **Figure 2 – figure supplement 1**

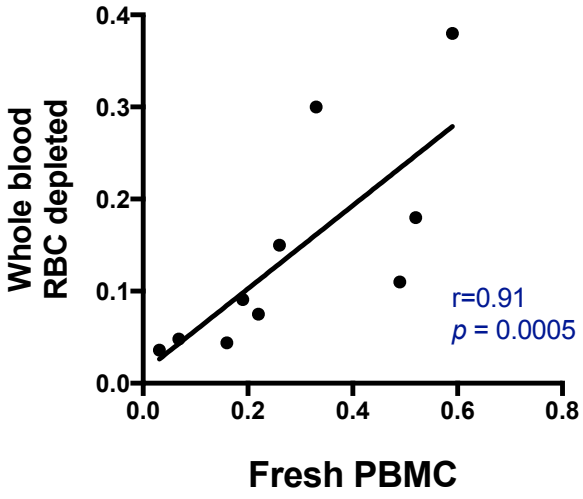

709

710

711 **Figure 2 – figure supplement 2**

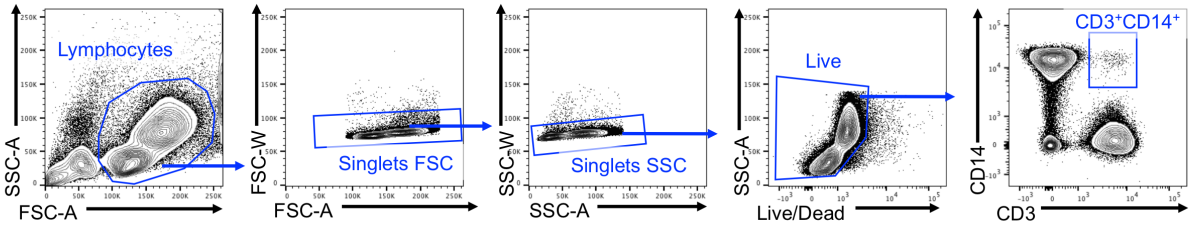

712

713

714 **Figure 2 – figure supplement 3**

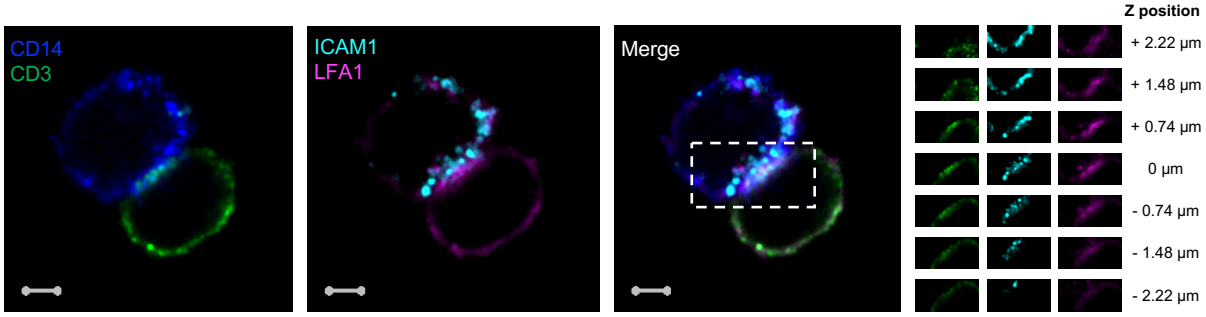

715

716 **Figure 3**

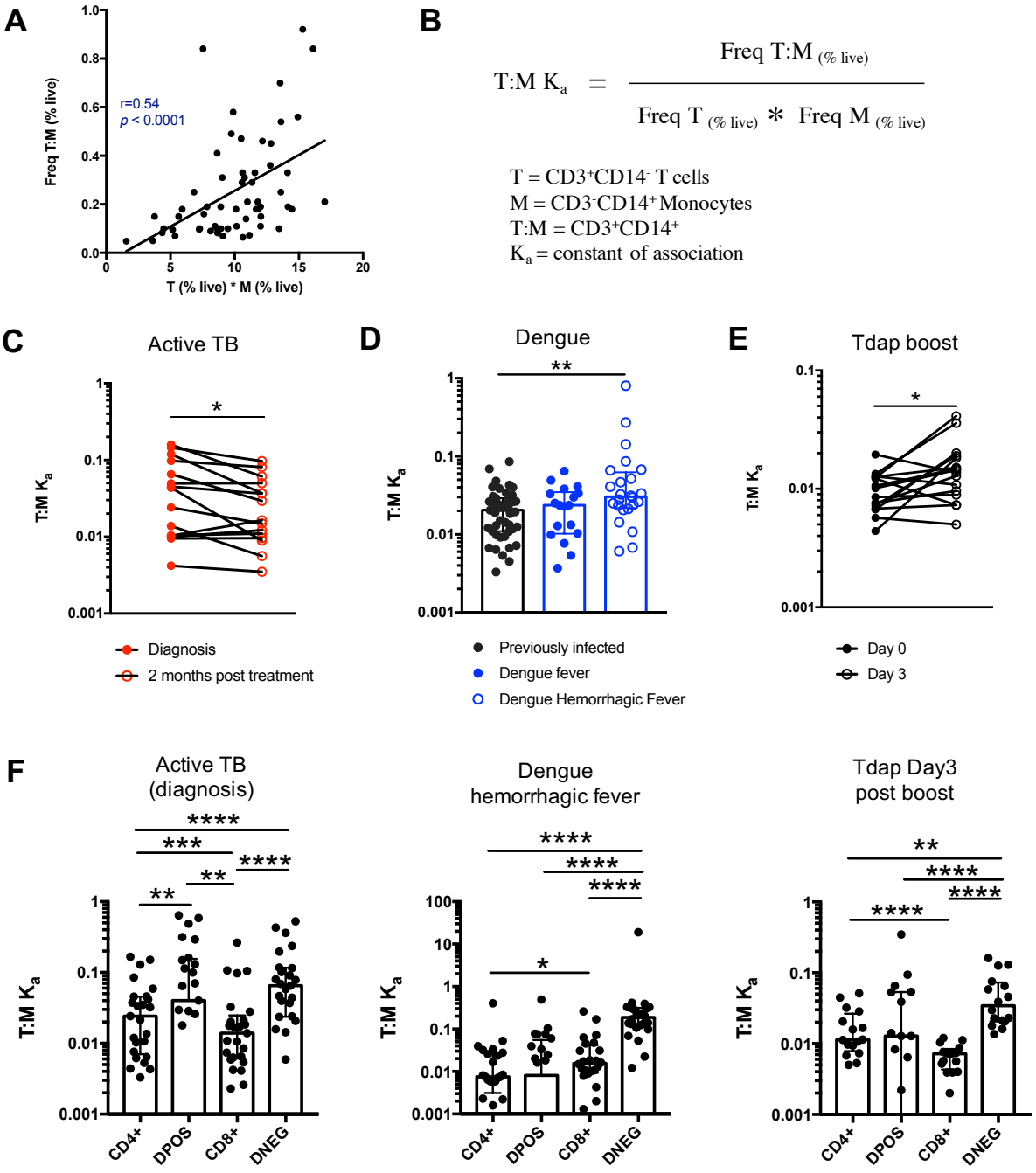

717

718

719 **Figure 3 – figure supplement 1**

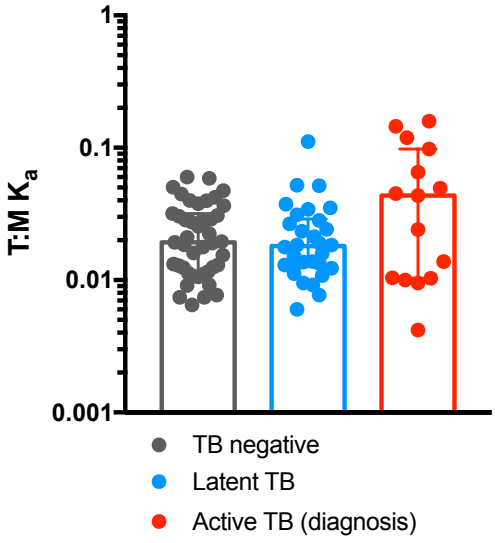

720

721

722 **Figure 3 – figure supplement 2**

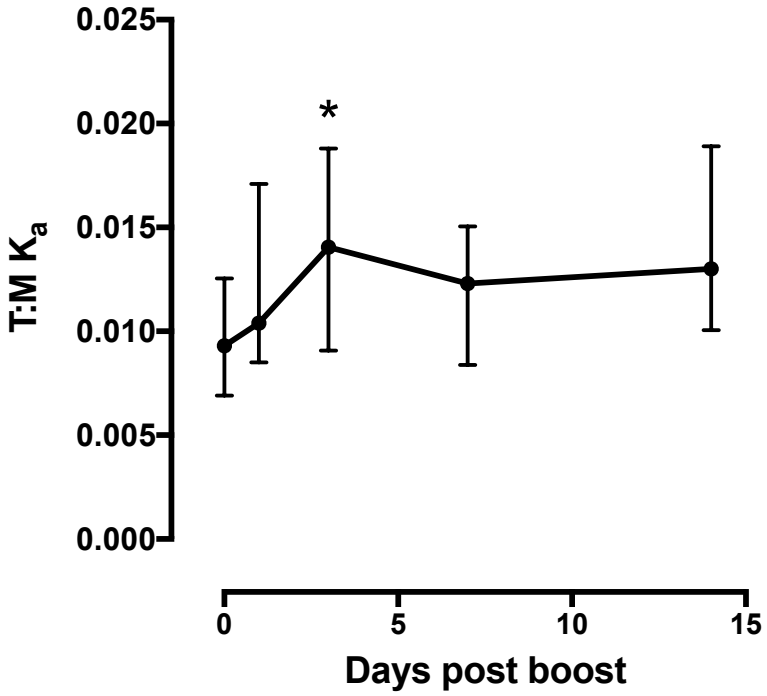

723

724

725 **Figure 3 – figure supplement 3**

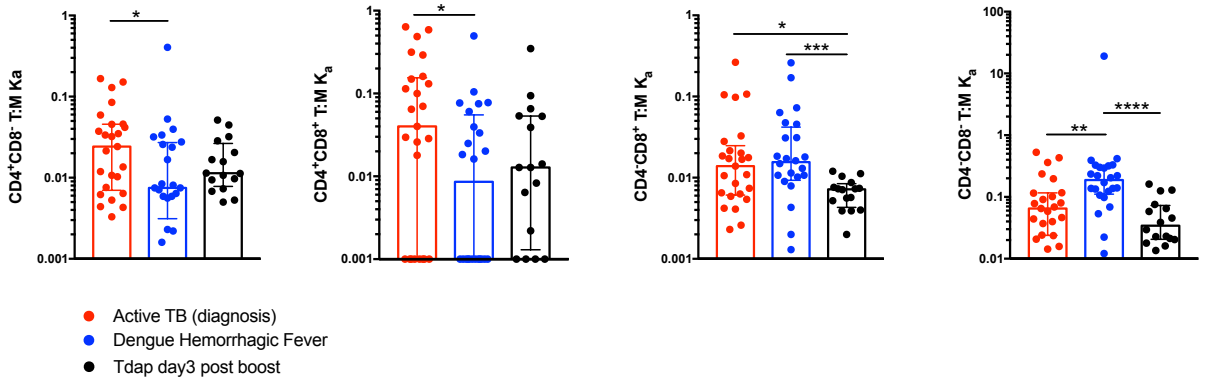

726

727

728 **Figure 3 – figure supplement 4**

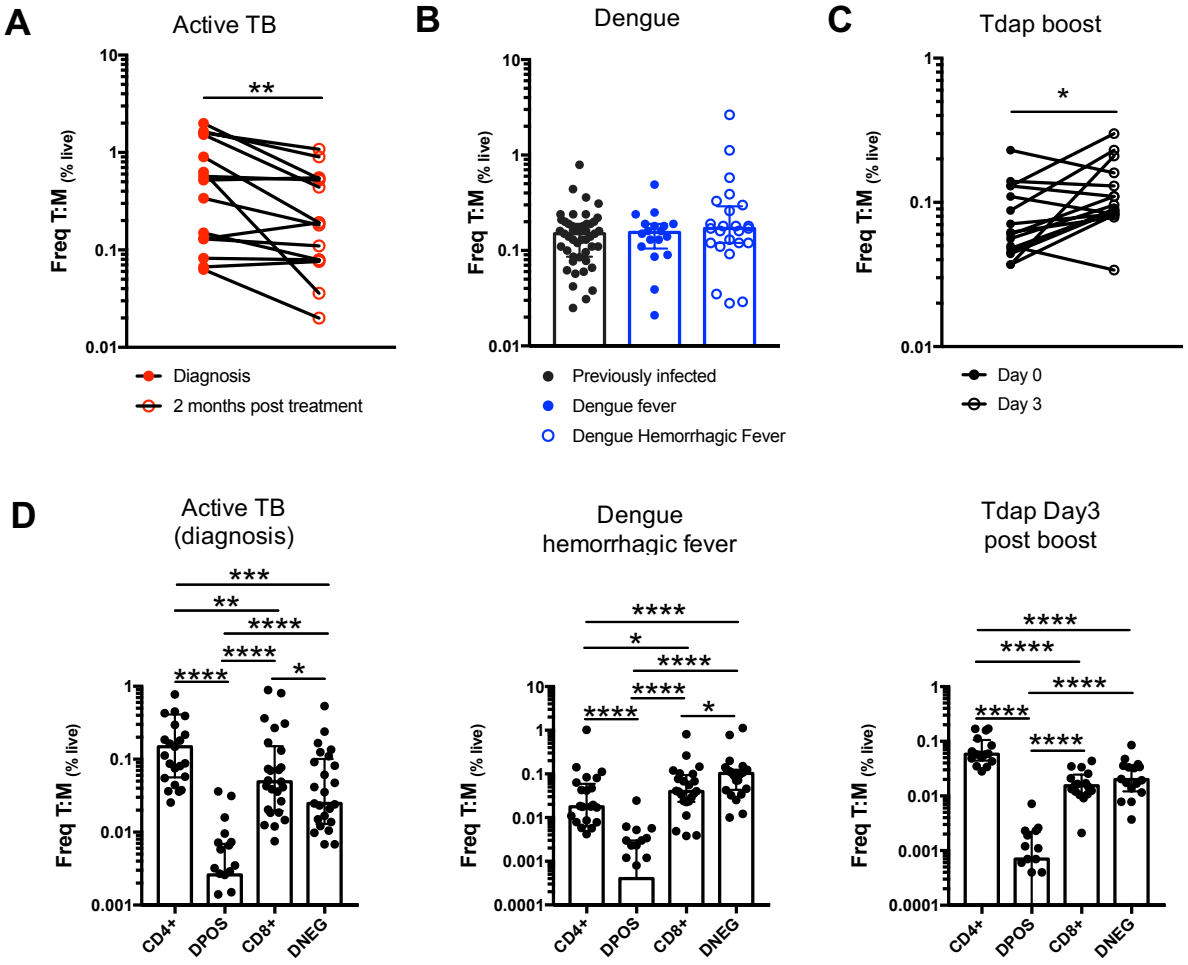

729